School of Engineering

Master of Mechanical and Aerospace of Engineering

Nazarbayev University

53 Kabanbay Batyr Avenue,

Astana, Kazakhstan, 010000

CFD MULTIPHASE MODELING OF BLOOD CELLS SEGREGATION IN FLOW THROUGH MICROTUBES

Anuar Ormanaliyev, B. Eng and Technology

Supervisor: Luis R. Rojas-Solórzano

Co-supervisor: Konstantinos Kostas

December 2018

Abstract

Development of a proper blood damage model is important step in future evolution of the blood wetted devices. The mentioned model on the other hand, requires an accurate blood cell segregation prediction. Blood segregation is a phenomenon when the red blood cells tend to concentrate at the bottom and center regions of the pipe, driving the platelets to concentrate at the upper wall region of the tube. In general, the segregation of the blood is found experimentally, although these experiments were found to be costly and time intensive. Development of a numerical model for blood segregation with help of Computational Fluid Dynamics has a potential to be fast and cheap alternative to the experiments. Previous works on blood cell segregation model of Mendygarin et al [4] and Supiyev et al [6] have followed the general pattern of the blood cells migration inside the tube, though they underpredicted the peak concentration of platelets near the wall. This Master thesis work will try to improve the numerical model of the predecessors by considering the lift force and virtual mass force. Lift force plays essential role in the region near the wall, since it drives the particles from the wall towards the centerline of the tube due to vorticity effects. It is assumed that red blood cells will experience higher lift force due to the larger size compared to platelets and will force the latter to migrate towards the wall region. This mechanism will be used to improve the prediction of the platelets peak.

Acknowledgements

Firstly, I would like to express the deepest appreciation to my supervisor Luis R. Rojas-Solórzano and co-supervisor Konstantinos Kostas. I would like to express utmost thankfulness for all the help, guidance, patience and discussions they offered during the thesis work. The completion of the thesis work would be impossible without huge support provided by them. It has been their supervision and direction, stimulating my suggestions and encouragement throughout the duration of my studies which has allowed me to successfully complete the Master's program.

Secondly, I would like to show my appreciation to the School of Engineering and especially Department of Mechanical and Aerospace Engineering stuff that gave me important knowledge and advices in my sphere during the Master's program.

Finally, I would like to thank my parents and my relatives for all support.

Outline

List of Abbreviation & Symbols

ρ_{rbc}	Density of the RBC
ρ_{plt}	Density of the PLT
ρ_{pl}	Density of the plasma
c_d	Drag coefficient
ε_{pl}	Volume fraction of plasma
ε_{rbc}	Volume fraction of RBC
ε_{plt}	Volume fraction of PLT
$\vec{v}_{pl}$	Velocity of plasma vector
$\vec{v}_{rbc}$	Velocity of RBC vector
$\vec{v}_{plt}$	Velocity of PLT vector
$\vec{g}$	Gravitational acceleration
∇P	Pressure gradient
∇P_{pl}	Plasma pressure gradient
∇P_{rbc}	RBC pressure gradient
∇P_{plt}	PLT pressure gradient
$\vec{\tau}_{pl}$	Plasma stress tensor
$\vec{\tau}_{rbc}$	RBC stress tensor
$\vec{\tau}_{plt}$	PLT stress tensor
β	Drag exchange coefficient
θ	Granular temperature
$\vec{I}$	Unit tensor
k	Granular conductivity
k_{rbc}	RBC extinction coefficient of the absorbing medium
k_{plt}	PLT extinction coefficient of the absorbing medium
γ	Energy dissipation
d_p	Diameter of particle
$\nabla \cdot \vec{\tau}_f$	Divergence of the stress tensor of the plasma
$\nabla \cdot \vec{\tau}_r$	Divergence of the stress tensor of RBC
$\nabla \cdot \vec{\tau}_s$	Divergence of the stress tensor of platelet
θ	Granular temperature
γ	Energy dissipation due to inelastic collision of particles
μ_f	plasma viscosity

μ_r	RBC viscosity
μ_s	platelet viscosity
ξ_f	bulk viscosity of plasma
ξ_r	bulk viscosity of RBC
ξ_s	bulk viscosity of PLT

List of Tables

List of Figures

Chapter 1 - Introduction

1.1. General information

Cardiovascular diseases (CVD) affect blood circulation system namely heart, veins, capillaries and arteries. They are the leading cause of death worldwide, and according to Worth Health Organization report, in 2015, CVD led 17.7 million death worldwide. [1] Preventive measure such as healthy lifestyle, hygiene, and healthy food, for example, may reduce the chance of CVD. However, in many cases, surgical treatment is the measure utilized to save the patient. Special devices, called blood-wetted devices are required in some treatments to provide proper blood circulation and pressure. The problem with these devices is that blood flowing through them can be damaged due to different biomechanical properties of the device walls. Different shear stresses cause the red blood cells to change their shape, damage and lead to hemolysis.

Hemolysis is the disruption of RBC membranes, which contributes to the release of hemoglobin stored in the erythrocytes [2]. Hemolysis has adverse effects on health, such as vascular dysfunction, injury, and inflammation. [3]

The leading cause of hemolysis is the high shear rate in blood flow through medical devices. Many experiments were done, and the behavior of the blood cells inside capillary and micro-tubes is well investigated. However, accurate data requires in-vitro experiments or experiments with animal or human blood leading to ethical constraints. A potential alternative solution is the usage of Computational Fluid Dynamics (CFD) techniques. CFD has potential to substitute experiments, though the current state of the CFD multiphase modeling still lies far from the experimental results. This study aims to improve the blood segregation model developed by Mendygarin et al. [4] as an attempt to develop further blood trauma models where every cell location is well predicted.

The model here proposed will be a scale-up of the previous model by Mendygaryn et al. [4], by considering the presence of lift and virtual mass forces (VMF).

Development of the improved model is essential, as proper blood cell segregation model offers real hope for blood cell damage (hemolysis) modeling in the near future, perhaps via CAE optimization.

1.2. Aims and objectives

The aim of this study is the enhancement of the existing blood cell segregation model developed in the Eulerian-Eulerian framework. The model has the potential to be base for future blood cell damage model, and it is vital to capture

the segregation accurately in order to simulate blood cell trauma in medical devices.

The particular objective is to improve and validate the current blood segregation model under the effects of virtual mass and lift forces on the prediction of the maximum PLT concentration near the wall of a capillary tube. This model will be assessed in several manners:

- examine the effect of each force separately and
- examine the cumulative effect of the lift and virtual mass forces

1.3. Methodology

During this thesis work, blood will be simulated as a Newtonian fluid made of plasma and two sets of rigid particles: red blood cells (RBC) and platelets (PLT). The particle distribution and inter-relation inside the tube will be simulated using the finite volume method and existing Eulerian-Eulerian multiphase CFD model developed by Mendygaryn et al. [4]. in the platform ANSYS-Fluent. In addition, Granular Kinetic Theory (GKT) will be used for different interrelations between the main phase (plasma) and dispersed phase (RBCs and PLTs). Granular Kinetic Theory was proven to be accurate in predicting pressure distribution and particle concentration in slurry flows. The GKT considers frictional, collisional and dynamic effects that occur between the main phase and dispersed phases.

Blood segregation model is based on an effect known as Fahraeus-Lindquist (F-L) effect. In very small tubes (diameter < 300 μm) flow resistance tends to decrease, driving the heavier RBC to move towards the center of the tube, forcing PLTs to concentrate near the wall [5]. This work is highly interested in predicting the peak PLT concentration near the wall caused by F-L effect.

Initial blood segregation model developed by Mendygarin et al. [4] assumed PLTs and RBC to be ideal spherical bodies. Later, Supiyev et al. [6] hypothesized that shape deformation of the RBCs and thus, changing drag coefficient, should improve the PLTs peak prediction. According to Supiyev et al.'s [6] hypothesis, different drag force developed according to the shape of the RBC at the flow regime should improve the model capabilities. However, their results proved that shape deformation did not improve peak PLT prediction in the capillary tube domain as observed in experiments.

Consequently, this work will be based on the initial model of Mendygaryn et al. [4], without changing the shape of the RBC. The main focus of this work will be observation of the lift force and virtual mass force effects on predicting the peak concentration of the PLTs near the wall. Inertial lift forces developed in an asymmetric flow appeared to be important in regions with high shear, thus, with lower drag. They move the particles towards the centerline of the tube. The magnitude of the mentioned lift force depends on a square of the particle diameter. It is assumed that lift forces acting on a larger size RBCs will move

them from the wall, increasing the local concentration of the PLTs. Besides, the effects of the VMF are assumed to be much smaller compared to the lift force. It is predicted that lift force will be the main force driving the RBC to the tube centerline, VMF is included as an additional observation force.

1.4. Structure of the thesis

This work will be divided into the following sections:

- literature review on previous blood segregation models and simulations as long as the description of the lift and virtual mass force models chosen for this study
- methodology and implementation of the model
- Results and discussion as well as conclusions and future work

Chapter 2 – Literature Review

This section of the report will present the experiments done by predecessors on blood segregation model, underlying mechanisms and importance of the VMF and lift forces for chosen simulation set up as well as mathematical model descriptions for lift coefficient.

2.1. Models of blood cells spatial distribution in flow through tubes

2.1.1. Experiment of the Yeh et al. [7]

Experiments on Fahraeus-Lindquist effect have been done by many research groups. This thesis will consider the experiment and results presented by Yeh et

al. [7], as the benchmark. In their experiment, they took the tube of diameter 217 μm, filled with plasma mixed with RBC and latex beads (they were used instead of PLTs). The concentration of RBC was set at 40%, and a number of latex beads were between 170 000-220 000 per mm3 representing a volumetric concentration near 2%. After mixing, introducing a homogeneous fluid, letting it flow through the capillary tube, and letting it reach a steady state, the tube was frozen. PLT concentrations at a different distance from the center were quantified by a microscope-based technique. It was found that PLTs and RBCs segregate and there is a peak of PLT relative concentration about 11 very near the tube wall as shown in Figure 2.1.1.

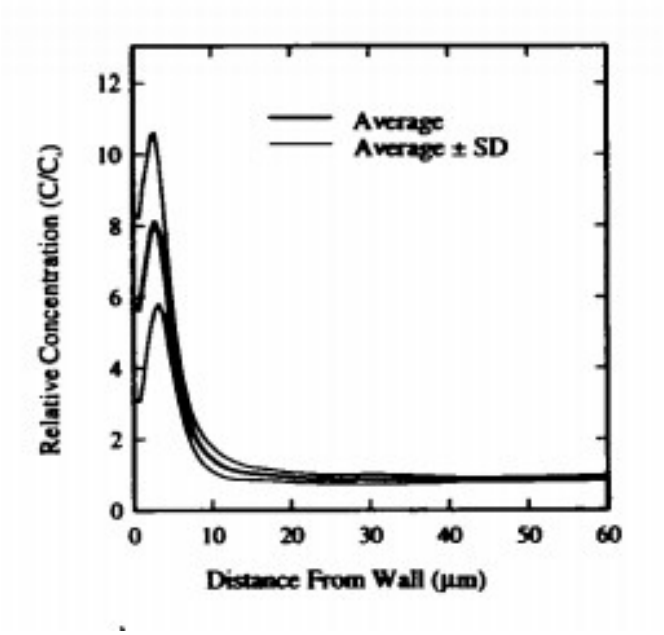

Figure 2.1.1. Peak Platelet concentration inside the tube (Yeh et al. [7])

2.1.2. Blood segregation model by Mendygarin et al. [4]

In 2016, Mendygarin et al [4] presented their CFD model to predict blood cells segregation. Their model considered Eulerian-Eulerian multiphase model, with 3 phases (plasma, RBC and PLT), and was based on Granular Kinetic Theory (GKT) to model the viscosity of the particles. In their simulations, RBCs and PLTs were assumed as spherical rigid bodies. The model included RBC-plasma and PLT-plasma interfacial forces. The resultant PLT distribution along the tube was similar to one obtained by Yeh et al., though the PLT peak was about 6 times smaller. The results obtained by Mendygarin et al [4] are shown in the following figure:

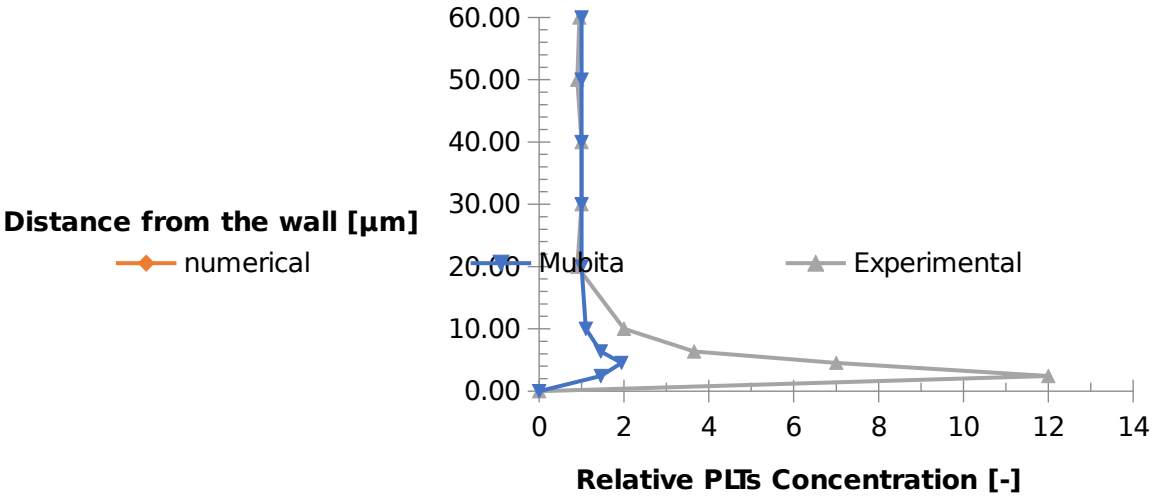

Figure 2.1.2. Results of the peak PLT concentration inside the tube (Mendygarin et al [4])

2.1.3. Blood segregation model by Supiyev et al. [6]

In 2017, Supiyev et al. developed their model aiming to improve the peak PLT concentration found in Mendygarin et al [4] work by considering shape

deformation of the RBCs inside the flow under different Reynolds number regimes. Depending on the shape of the deformed RBC, drag coefficient and Reynolds number were adjusted in the interfacial forces between RBC and plasma and thereafter, peak PLT concentrations were determined following the same protocol presented in Mendygarin et al [4] to match Yeh et al.'s [7] results. The results did not show any progress as shown in fig. 2.1.3, so it was concluded that the shape of the RBC does not affect the segregation significantly.

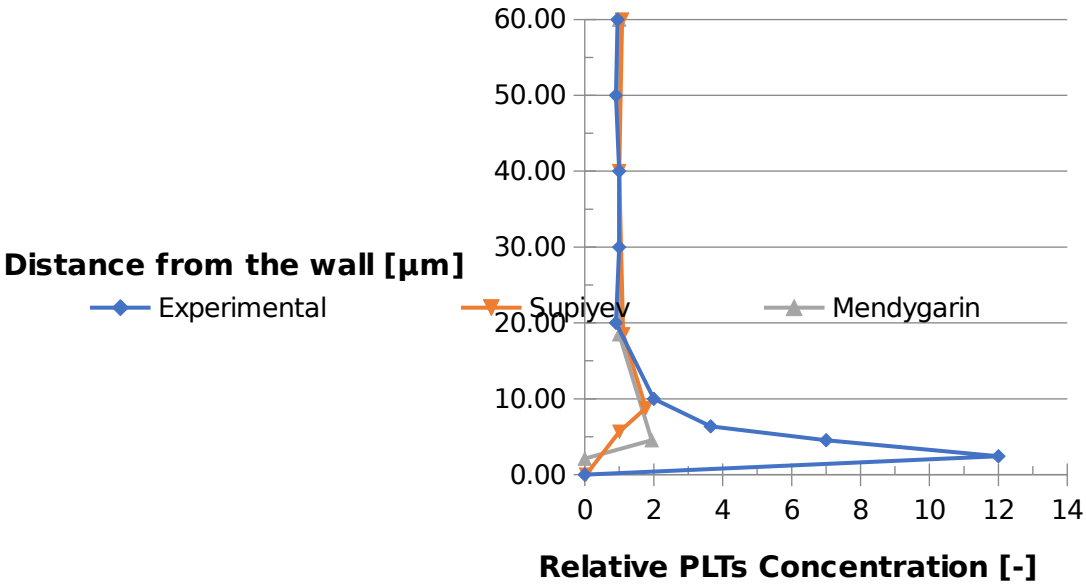

Figure 2.1.3. Results of the peak PLT concentration inside the tube (Supiyev et al [6])

2.2. Forces affecting particle inside asymmetric flow

According to Kolev [8] the symmetric particle(sphere) exposed to asymmetric flow experiences the following forces: drag, VMF and lift. The Figure represents the direction of the mentioned forces:

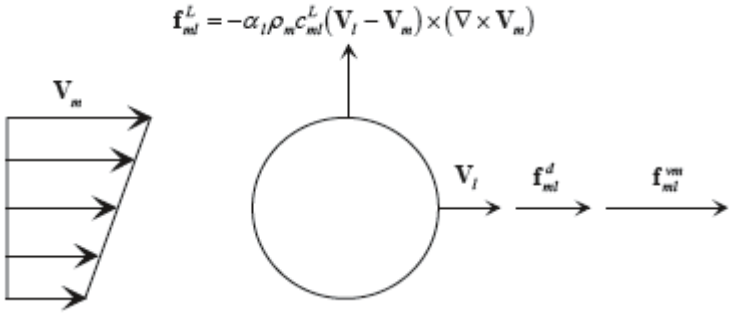

Figure 2.2 Drag, virtual mass, and lift forces acting simultaneously on the field (Kolev et al [8]).

This thesis will simulate the experimental conditions of the Yeh et al.: horizontal flow of the particles inside the cylindrical tube. In this case, the flow will be asymmetrical due to the presence of the gravity force. Thus, the particles inside the tube will be affected by drag, VMF and lift forces.

In next sections of the literature review the nature of the VMF and lift force, a theory describing the importance of the forces in asymmetric flow, experiments were done to demonstrate the effects of the abovementioned forces on particle distribution inside the tube and description of the mathematical models used for simulation will be discussed.

2.2.1. Lift force description and importance

2.2.1.1. Lift Forces general description

Zhou et al. [9] state that particles flowing through microchannel are mainly affected by two dominant forces: viscous drag and inertial lift force. Last one forces particles to move across the streamlines.

There are three types of lift force inside the tube; shear-induced lift force, which drives the particles toward the channel walls, wall-induced lift force, which moves them out from the wall and acts up to velocity gradient and rotation-induced lift, which lead the particles toward wall center. In radially symmetric channel (capillary or tube channels) migration of the particles occurs without rotation induced lift force.

At low Reynolds number effect of the rotational-induced lift force is very small compared to wall-induced lift force [10]. It was rechecked by Zeng et al. [10] in his work and described by many previous works.

Besides, Zeng et al. [10] state that for $Re < 100$, they observed the lift coefficient to decrease with both Reynolds number and distance from the wall.

Zeng et al. [10] mention that the wall-induced lift force is due to two competing mechanisms. First, the vorticity generated at the surface of the particle advects and diffuses downstream. Because of a nearby wall, axisymmetry of the wake vorticity distribution breaks. The resulting induced velocity also breaks the symmetry and results in an effective lift force that tends to move the particle away from the wall. Second, from inviscid theory, one can argue that the flow relative to the particle will accelerate faster in the gap between the particle and the wall. The resulting low pressure in the gap will induce a lift force directed toward the wall.

Takemura and Magnaudet [11] states that the 1st lift mechanism will dominate the second in the case if the Reynolds number is less than unity and for solid particles the domination of the vorticity induced lift force will be dominant for a moderate (1<Re<100) Reynolds number.

Reynolds number was found to be affecting the migration of the particles. For a very low Re (Re<10-6) no migration of the rigid particles is observed [12]. In this thesis work the magnitude of the Re is greater than the mentioned threshold (values for Re for RBC and PLT will be shown later in methodology part of the thesis) and thus, the migration assumed to be present.

The particle inside the flow will be affected by different lift force depending on its velocity. If the particle lags the fluid, the lift will move the particle toward the faster adjacent fluid and vice versa if the particle leads the fluid [13].

Particles located at high shear rate regions are more mobile, and drag effects acting on them are lower compared to low shear region particles. According to Al Taweel et al. [14] lift force plays an essential role at high shear rates and low concentrations. To be more precise, in regions with high shear, lift force dominates the viscous drag force.

From the review of the lift force acting on a particle inside the multiphase flow, we can observe the importance of the lift force in the region near the wall. This thesis work aims to implement the lift force modelling and observe the effect of the lift force on blood cell segregation.

2.2.1.2. Non-inertial lift forces

In addition to inertial lift forces, non-inertial forces are acting on a deformable object such as droplets. Goldsmith and Mason [13] found that deformable objects are affected by lift force at very low Re (<10-6), while rigid solid particles are not. From their experiment, they concluded the presence of non-inertial lift forces. This thesis work assumes the RBC and PLTs to be sphere like rigid particles and thus, the effects of the non-inertial forces are equal to 0. However, the consideration of the mentioned forces might be important for future studies that will consider the deformation of the RBCs inside the flow.

2.2.1.3. Effect of the lift force on RBCs volume distribution

One experiment demonstrating the effect of the lift force on RBC distribution in the horizontal tube is the experiment Massoudi et al. [15] was testing effects of the different parameters such as Reynolds number, drag and lift coefficients on RBC velocity and volume fraction distribution. In their work, they assumed the blood to be 2 phase fluid consisting of plasma and RBC flowing between 2 horizontal flat plates. Plasma was chosen to behave as viscous fluid whereas RBC was given a granular-like structure with variable viscosity depending on the shear rate. The approximations used in the work is the same as used in this MSc thesis. The following figure illustrates the RBC volume fraction

distribution for different lift coefficients.

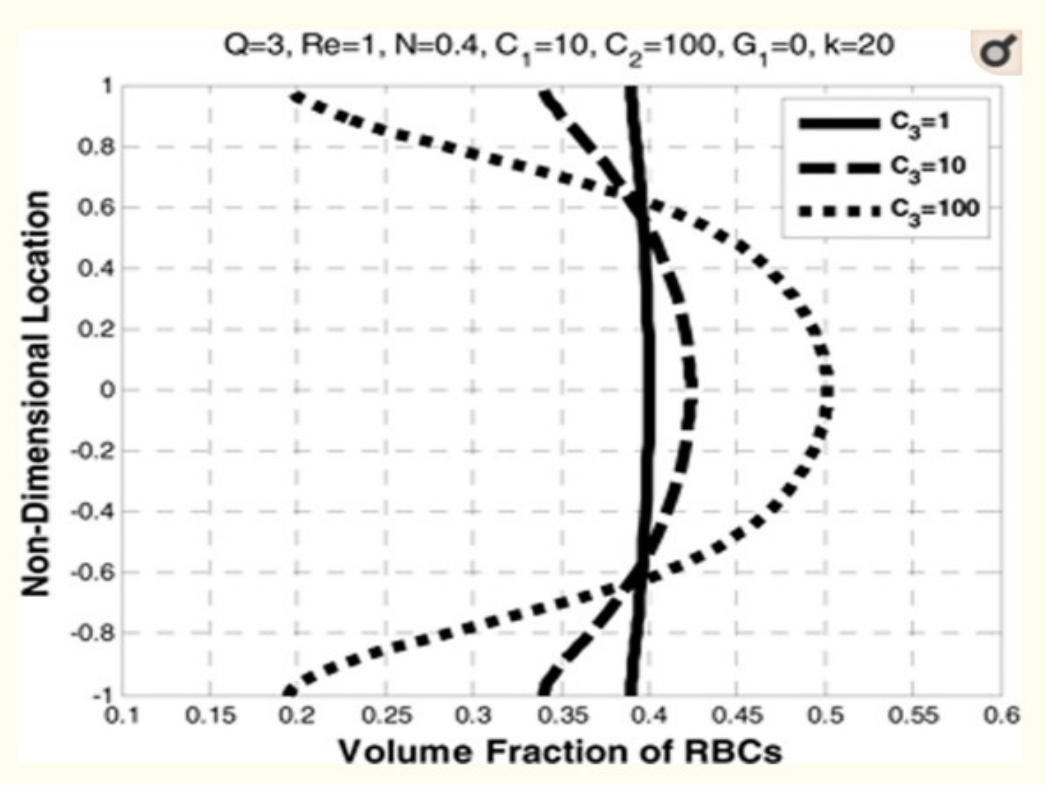

Figure 2.2.1.3. Effect of lift coefficient (C3) on the volume fraction of RBCs (Massoudi et al [15])

From the figure, we can observe that RBCs are moved to the center with higher lift forces. Although in this thesis work lift coefficient will not be a constant value of that high magnitude, the evidence of the RBC migration towards the center because of lift force is substantial.

2.2.2. General theory behind VMF

It was previously stated that the main forces acting on a particle in microtubes are drag and lift forces. It is hypothesized that the lift force will be the main driving force in particle migration. Nevertheless, this thesis work also will examine the influence of the VMF on blood cell segregation.

In the following paragraph of this section, the virtual mass concept is described in order to familiarize the reader with its nature and implications before it is implemented in this thesis report.

When a given body moves inside any continuum medium the body experiences a virtual mass force that increases the mass of the body [8].

Lamb [16] computed the virtual mass coefficient for a particle in potential

flow with ellipsoidal shape defined by:

$$f_d^{v_m} = -\alpha_d R c_d^{vm} \left[\frac{\partial}{\partial \tau} \Delta V_{cd} + \left(v_d \nabla \right) \Delta v_{cd} \right]$$

(1)

,where ∇V_{cd} velocity difference continuous minus disperse, α_d particle volume fraction, c_d^{vm} virtual mass force coefficient for the force acting on the dispersed field which is submerged into the continuous field c.

The virtual mass force is experienced by the body as if it had an additional mass during its translation relative to the continuum phase (plasma). This explains the other name sometimes used for this force, “added mass force”. For larger particle concentrations, v_m d c is a function of α.

$$\frac{x^2}{R_x}+\frac{y^2}{R_y}+\frac{z^2}{R_z}=1$$

(2)

where the lengths of the principal axes are R_x, R_y and R_z , and the relative velocity is parallel to the x-axis as follows (see Table 2.2.2):

$$c_{cd}^{vm}=\frac{a_0}{2-a_0}$$

(3)

$$a_0=R_x R_y R_z \int_0^{\infty} \frac{d\lambda}{\left(R_x^2+\lambda\right)\left(R_y^2+\lambda\right)\left(R_z^2+\lambda\right)} \qquad (4)$$

Table 2.2.2. Virtual mass coefficients for an ellipsoid (Bournaski et al [17])

Shape of particles	Translation parallel to axis		
	x	y	z
	$c_{cd,x}^{vm}$	$c_{cd,y}^{vm}$	$c_{cd,z}^{vm}$
$R_x = R_y = R_z$, sphere	1/2	1/2	1/2
$R_x = R_y = R_z/2$, rotary ellipsoid	0.704	0.704	0.210
$R_x = R_y = R_z/3$, rotary ellipsoid	0.803	0.803	0.122
$R_x = R_y = R_z/4$, rotary ellipsoid	0.859	0.859	0.081
$R_x = (2/3)R_y = R_z/2$, unrotary ellipsoid	0.936	0.439	0.268
$R_x = R_y/2 = R_z/4$, unrotary ellipsoid	1.516	0.398	0.126

In the model developed in this investigation, RBCs and PLTs are assumed to be ideal spherical bodies and Rx=Ry=Rz=0.5. Thus, the virtual mass coefficient is 0.5 for upcoming simulations.

The experiments show that if spheres(particles) are separated by 3 or more radii (the radii of the particle), then the virtual mass coefficient remains at the value of 0.5 [18]. That value will be chosen for the simulation.

Since the density difference between RBC and plasma is 7.3% and PLT and plasma 1.46%, this thesis assumes the effect of the virtual mass to be much lower, or almost negligible compared to the impact of the lift force. Nevertheless, the author wants to observe the effect of the VMF paired with lift force at very low drag.

2.3. Lift models

2.3.1. Selection of a lift model

Now, when the basic physics of the VMF and lift forces are described, there is a necessity in the selection of a proper lift and VMF models. For VMF a constant coefficient will be applied.

On the other hand, the use of a constant lift coefficient will be inappropriate and vague assumption due to particle migration inside the tube caused by both viscous and inertial effects. Consequently, a separate section of the literature review will be dedicated to the selection of a proper lift model.

According to Yilmaz and Gundogdu's [19] review the parameters affecting the lift force magnitude are: relative velocity produced between fluid and particle, a rotational speed of the particle, boundary conditions of the surface and shear rate of the fluid.

In addition, from the definition of the multiphase flow, it is known that one phase will have relative motion with respect to other phases. The number of phases affects the number of velocity fields, for instance, the two-phase flow problem will be developed concerning the two-velocity field.

Abovementioned factors cause the modeling process of the lift force to be a significant challenge [20], [21].

According to Geislinger's review [22] Saffman [23], [24] proposed the first theoretical description of the lateral migration of solid spheres due to the inertial effects of the fluid. The model assumed low Reynolds number and large shear in the tube.

2.3.2. Saffman's model description

In this model, lift force is caused by pressure distribution affecting the particle due to the rotation. The rotation is produced from the velocity gradient.

The solution is based on a matched asymptotic expansion. To be more precise, shear at the outer region produces inertial effects that modify the flow in the inner region. The common expression of the Saffman's model [23,24] is:

$$L = 1{,}615\,\rho_f\, v_f^{\frac{1}{2}} d_p^2 u_r \left|\frac{\partial u}{\partial y}\right|^{\frac{1}{2}} sign\left(\frac{\partial u}{\partial y}\right) \tag{5}$$

ρ_f and v_f – density and kinematic viscosity of the continuous phase, u and v – velocities of the continuous and dispersed phases in direction of the motion, d – diameter of the particle (particle assumed to be spherical) and $\partial u/\partial y$ – the shear rate of the uniform field . This model requires the particle's Reynolds number to be much less than shear Reynolds number, Re_G and both Reynolds numbers are expected to be much smaller than unity, and equal to:

$$\mu_c^{-¿} \ll 1 \qquad \mu_c^{-¿} \ll 1$$
$$\Re = \frac{|u-v|\,d}{v_c} = \frac{\rho_a u_r d}{¿} \quad ; \quad \Re = \frac{|du\,dy|\,d}{v_c} = \frac{\rho_a u_r d}{¿} \tag{6}$$

$$\beta = \frac{Re_G^{1/2}}{\Re} \gg 1; \tag{7}$$

It is well known that shear rate is low at the center of the tube and increases towards the wall.

The problem with the model is that it cannot be properly used for positions near the wall. This is due to the severe infringement of the local Reynolds number near the wall.

Next generation of researchers improved the model, and, in this thesis, the focus will be placed on the model improvement introduced by Mei [25].

2.3.3. Mei's model description

This model introduces the mathematical equations for lift coefficient for higher range of the particle's Reynolds number, namely for Re between 0.1 and 100 [25].

$$L=1{,}615\,\rho_f\,v_f^{\frac{1}{2}}\,d_p^2\,u_r\left\{\left(1-0.3314\,\square^{1/2}\right)\exp\left(\frac{-\Re}{10}\right)+0.3314\,\square^{1/2}\right\}\left|\frac{du}{dy}\right|^{\frac{1}{2}}sign\left(\frac{du}{dy}\right)$$

(8)

For Re $\leq$ 40 and;

$$L=1{,}615\,\rho_f\,v_f^{\frac{1}{2}}\,d_p^2\,u_r\,\text{¿}\,\{0.0524\,\text{¿}\,\Re\,\text{¿}\,\text{¿}1/2\}\left|\frac{du}{dy}\right| \qquad (9)$$

For Re $\geq$ 40.

Where finite shear rate is defined as:

$$\text{¿(¿¿2)/2}=\frac{\Re_G}{2\Re}=\left(\frac{d}{2}\right)^{\Re\,\beta}\left|\frac{du}{dy}\right|^{\text{¿}} / |u-y| \quad (10)$$

and the range is between 0.005 and 0.4.

The current equations were assumed for the constant velocity gradient and infinite flow field. If the size of the particle is much smaller than the tube diameter, these assumptions can be satisfied locally.

In the model presented in this investigation, the diameter of the tube (217 µm) is 36 times greater than the particle size (6µm).

In addition, the tube was chosen to be of cylindrical form without any curvatures and 100 cm long. The conditions for Mei's lift coefficient are satisfied under the condition of the chosen model and can be implemented for simulation.

Chapter 3 – Methodology and Simulation Setup

3.1. **Preamble**

A uniform velocity profile is prescribed for the blood flow at the entrance in the proposed model. The inlet flow for all phases to be 1.505×10^{-2} m/s in order to have all axial velocities equivalent to the Poisseuille wall shear rate 555 s^{-1} used by Yeh et al. [7]. The radial velocities are set to be zero. Later, velocity develops a parabolic profile, represented in Figure 3.1.1.

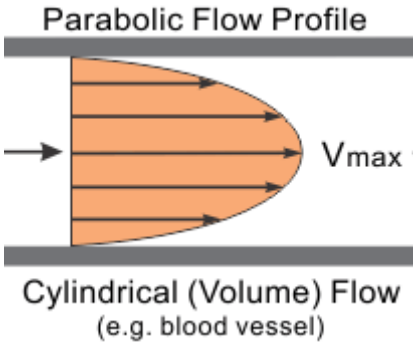

Figure 3.1.1.: Flow rate-driven flow (source: http://www.cvphysiology.com/Hemodynamics/H006 [26])

This simulation considers Eulerian-Eulerian multiphase model and mixture of plasma, RBC and PLT. Plasma is set as continuum phase, while RBCs with PLTs are dispersed phases. Length of the tube is 100mm with the diameter of 217µm.

The diameter of the tube was similar to the one prepared by Mendygarin et al. [4]. The tube was axis-symmetrical and 40 times greater than a diameter of the RBC. The geometry reproduces the experiment done by Yeh et al. [7], which in turn is used for validation purposes. Figure 3.1.2. shows a schematic of the computational domain tube with constant cross-section used by Yeh et al. [7]

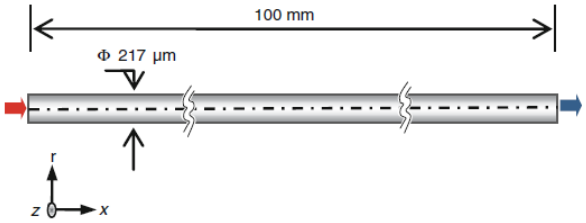

Figure 3.1.2. Computational domain tube (Yeh et al. [7])

Plasma was set to be Newtonian fluid. RBCs and PLTs are spherical solid particles. The viscosity of the dispersed phases will be calculated by GKT; thus, they are not fixed parameters and varies within the flow field. The granular temperature at the wall (boundary condition for GKT) for disperse phases was set to $10^{-8} m^2/s^2$.

3.2. Physical properties and numerical setup

Density, flow rate, volume fraction and Sauter diameters are defined and shown in Table 3.2.

Table 3.2: Flow parameters

Phase	**Plasma**	**RBC**	**PLT**
Density [kg/m^3]	1,025	1,100	1,040
Viscosity [kg/m*s]	0.0012	Found by GKT	Found by GKT

D_p (Sauter Diameter) [μm]	-	5.5	2.5
Volume Fraction [%]	58	40	2
Flow rate [cm/s]	1.505	1.505	1.505

Turbulence effects were not performed in this simulation because of low Reynolds number (Re<5) [3].

The calculation of the particle Re are shown in the following equations:

$$\Re_{rbc}\left(V=\frac{1.505\,cm}{s}\right)=\frac{1.505*10^{-2}*6*10^{-6}*1.1}{0.0012}=8.28*10^{-5}$$

$$\Re_{plt}\left(V=\frac{1.505\,cm}{s}\right)=\frac{1.505*10^{-2}*2*10^{-6}*1.040}{0.0012}=2.61*10^{-5}$$

These values are higher than the threshold determined by Goldsmith and Mason [10] and thus, lift force will be present at the simulation.

ANSYS FLUENT software will be used to examine the hypothesis presented earlier in the thesis.

Parameters as drag coefficient, restitution coefficient, packing limit and VMF coefficient will be constant.

The lift coefficient will not be at a fixed valued; saffman-mei lift model preinstalled in ANSYS FLUENT will be used to calculate the lift coefficient of each particle.

For VMF the constant coefficient 0.5 will be used for all simulations. In addition, implicit method and different implicit options will be used to increase the accuracy of the results.

VMF Implicit tool has three options: Default, Option 2 and Option 3. It is advised by ANSYS FLUENT user guide to use the Option at initial iterations to increase the convergence and then switch to the Default option. The same procedure will be applied in this thesis.

Drag coefficient CD will be constant for all simulations and will be equal to 1 and 5.5.

The conditions for simulation are the following:

- No stress condition at outlet boundary
- No-slip condition at the walls

The order of 10-8 is set for the accepted normalized errors, a convergence of momentum, volume fraction and granular temperature equations. QUICK solution method is applied to the spatial discretization of the convective term. All simulations were executed in ANSYS FLUENT platform under free Student version 19.2.

3.3. Mathematical model

Granular Kinetic Theory will be used to determine the viscosity of the dispersed phases. Gidaspow et al [27] introduced the main equations of the GKT.

First, the mass balance equations for the fluid (plasma) and solid (RBC and PLT) are described as follows:

Plasma mass balance:

$$\frac{\partial\left(\rho_{pl}\varepsilon_{pl}\right)}{\partial t}+\nabla\left(\rho_{pl}\varepsilon_{pl}\overrightarrow{v_{pl}}\right)=0 \tag{11}$$

RBCs mass balance:

$$\frac{\partial\left(\rho_{rbc}\varepsilon_{rbc}\right)}{\partial t}+\nabla\left(\rho_{rbc}\varepsilon_{rbc}\overrightarrow{v_{rbc}}\right)=0 \tag{12}$$

PLTs mass balance:

$$\frac{\partial\left(\rho_{plt}\varepsilon_{plt}\right)}{\partial t}+\nabla\left(\rho_{plt}\varepsilon_{plt}\overrightarrow{v_{plt}}\right)=0 \tag{13}$$

where ρ is density, t is time, ε is the volume fraction of each phase, and $\vec{V}$ is velocity.

Gidaspow et al. [27] states that mass balances differ from usual transport equations because of volume fraction consideration. Volume fractions may produce hydrodynamic forces, such that these forces may introduce clustering phenomena. The momentum balance equations are prescribed as:

Plasma momentum balance

$$\frac{\partial\left(\rho_{pl}\varepsilon_{pl}\vec{v}_{pl}\right)}{\partial t}+\nabla\left(\rho_{pl}\varepsilon_{pl}\overrightarrow{v_{pl}}\vec{v}_{pl}\right)=\rho_{pl}\varepsilon_{pl}\vec{g}-\varepsilon_{pl}\nabla P+\nabla\vec{\vec{\tau}}_{pl}+\beta\left(\vec{v}_{rbc}+\overrightarrow{v_{plt}}-\vec{v}_{pl}\right)$$

(14)

RBCs momentum balance

$$\frac{\partial\left(\rho_{rbc}\varepsilon_{rbc}\vec{v}_{rbc}\right)}{\partial t}+\nabla\left(\rho_{rbc}\varepsilon_{rbc}\overrightarrow{v_{rbc}}\vec{v}_{rbc}\right)=\rho_{rbc}\varepsilon_{rbc}\vec{g}-\varepsilon_{rbc}\nabla P-\nabla P_{rbc}+\nabla\vec{\vec{\tau}}_{rbc}+\beta\left(\vec{v}_{pl}+\overrightarrow{v_{plt}}-\overrightarrow{v_{rbc}}\right)$$

(15)

PLTs momentum balance

$$\frac{\partial\left(\rho_{plt}\varepsilon_{plt}\vec{v}_{plt}\right)}{\partial t}+\nabla\left(\rho_{plt}\varepsilon_{ptl}\overrightarrow{v_{ptl}}\vec{v}_{plt}\right)=\rho_{plt}\varepsilon_{plt}\vec{g}-\varepsilon_{plt}\nabla P-\nabla P_{plt}+\nabla\vec{\vec{\tau}}_{f}+\beta\left(\vec{v}_{pl}+\overrightarrow{v_{rbc}}-\overrightarrow{v_{plt}}\right)$$

(16)

where $\vec{g}$ is a gravity, P is a fluid pressure, P_{rbc} and P_{plt} are granular pressures, $\vec{\tau}_r$ is the stress tensor and β is the interface momentum-exchange coefficient.

The momentum balances are included to the ANSYS-FLUENT platform. These equations are stabilized by means of viscosity and pressure gradients.

Since it is a mixture, the sum of volume fractions must be equal to one:

$$\varepsilon_{pl}+\varepsilon_{rbc}+\varepsilon_{pl}=1 \tag{17}$$

Now, the Random Kinetic Energy (RKE) for the dispersed phases will be described.

RKE for RBCs:

$$\frac{3}{2}\left[\frac{\partial\left(\rho_{rbc}\varepsilon_{rbc}\theta\right)}{\partial t}+\nabla\left(\rho_{rbc}\varepsilon_{rbc}\theta\,\overrightarrow{v_{rbc}}\right)\right]=\left(-P_{rbc}\vec{\vec{I}}+\vec{\vec{\tau}}_{rbc}\right):\nabla\vec{v}_{rbc}+\nabla\left(k_{rbc}\nabla\theta\right)-\gamma$$

(18)

RKE for PLTs:

$$\frac{3}{2}\left[\frac{\partial\left(\rho_{plt}\varepsilon_{plt}\theta\right)}{\partial t}+\nabla\left(\rho_{plt}\varepsilon_{plt}\theta\,\overrightarrow{v_{plt}}\right)\right]=\left(-P_{plt}\vec{\vec{I}}+\vec{\vec{\tau}}_{plt}\right):\nabla\vec{v}_{plt}+\nabla\left(k_{plt}\nabla\theta\right)-\gamma \quad (19)$$

, where k is the granular conductivity, γ is the collisional dissipation and θ is the granular temperature. In GKT, granular temperature is the main force responsible for particle migration and is a measure of the random particle kinetic energy per unit mass. Viscous type dissipation is a main producer of the granular temperature and consumed due to inelastic collisions.

Newtonian type viscous approximation will be applied to define the stress tensor. The approximations are:

$$\vec{\vec{\tau}}_{pl}=\varepsilon_{pl}\mu_{pl}\left(\nabla\vec{v}_{pl}+\nabla\overrightarrow{v^{T}}_{pl}\right)-\frac{2}{3}\varepsilon_{pl}\mu_{pl}\nabla\vec{v}_{pl}\vec{\vec{I}} \quad (20)$$

$$\vec{\vec{\tau}}_{rbc}=\mu_{rbc}\left(\nabla\vec{v}_{rbc}+\nabla\overrightarrow{v^{T}}_{rbc}\right)+\left(\xi_{rbc}-\frac{2}{3}\mu_{rbc}\right)\nabla\vec{v}_{rbc}\vec{\vec{I}} \quad (21)$$

$$\vec{\vec{\tau}}_{plt}=\mu_{plt}\left(\nabla\vec{v}_{plt}+\nabla\overrightarrow{v^{T}}_{plt}\right)+\left(\xi_{plt}-\frac{2}{3}\mu_{plt}\right)\nabla\vec{v}_{plt}\vec{\vec{I}} \quad (22)$$

RBC pressure, P_s, shear viscosity, μ_s , and bulk viscosity, ξ_s , are expressed as a function of granular temperature based on the kinetic theory model.

$$P_{rbc}=\rho_{rbc}\varepsilon_{rbc}\theta+2\rho_{rbc}(1+e)\varepsilon^{2}_{rbc}g_0\theta \tag{23}$$

$$\mu_{rbc}=\frac{4}{5}\varepsilon^{2}_{rbc}\rho_e d_p g_0(1+e)\left(\frac{\theta}{\pi}\right)^{\frac{1}{2}}+\frac{10\rho_{rbc}d_p\varepsilon_{rbc}\sqrt{\theta\pi}}{96(1+e)g_0}\left[1+\frac{4}{5}\varepsilon_{rbc}g_0(1+e)\right]^{2} \tag{24}$$

$$\xi_{rbc}=\frac{4}{3}\varepsilon^{2}_{rbc}\rho_{rbc}d_p g_0(1+e)\left(\frac{\theta}{\pi}\right)^{\frac{1}{2}} \tag{25}$$

Same equations are applied for PLTs:

$$P_{plt}=\rho_{plt}\varepsilon_{plt}\theta+2\rho_{plt}(1+e)\varepsilon^{2}_{plt}g_0\theta \tag{26}$$

$$\mu_{plt}=\frac{4}{5}\varepsilon^{2}_{plt}\rho_{plt}d_p g_0(1+e)\left(\frac{\theta}{\pi}\right)^{\frac{1}{2}}+\frac{10\rho_{plt}d_p\varepsilon_{plt}\sqrt{\theta\pi}}{96(1+e)g_0}\left[1+\frac{4}{5}\varepsilon_{plt}g_0(1+e)\right]^{2} \tag{27}$$

$$\xi_{plt}=\frac{4}{3}\varepsilon^{2}_{plt}\rho_{plt}d_p g_0(1+e)\left(\frac{\theta}{\pi}\right)^{\frac{1}{2}} \tag{28}$$

where g_0 is the radial distribution function, d_p is the diameter of the particle and *e* is the restitution coefficient, which is a measure of the elasticity of the particle-particle collision. It is defined as the ratio of rebound velocity of particle to its velocity before impact.

Bagnold's equation [26] is used to express the radial distribution function, which express the statistics of the spatial arrangement:

$$g_0=\left[1-\left(\frac{\varepsilon_{plt}}{\varepsilon_{plt,max}}\right)^{1/3}\right]^{-1} \tag{29}$$

$$g_0=\left[1-\left(\frac{\varepsilon_{rbc}}{\varepsilon_{rbc,max}}\right)^{1/3}\right]^{-1} \tag{30}$$

To define the thermal conductivity, 2 components are introduced. First part (kinetic) is taken from the dilute kinetic theory of gases. Second one (collisional) is produced from inelastic collision of the particles. The final equation is the following:

$$k_{plt}=\frac{150\,\rho_{plt}\,d_p\,\varepsilon_{plt}\sqrt{\theta\pi}}{384(1+e)g_0}\left[1+\frac{6}{5}\varepsilon_{plt}\,g_0(1+e)\right]^2+2\varepsilon^2{}_{plt}\,\rho_{plt}\,d_p\,g_0(1+e)\left(\frac{\theta}{\pi}\right)^{\frac{1}{2}} \tag{31}$$

$$k_{rbc}=\frac{150\,\rho_{rbc}\,d_p\,\varepsilon_{rbc}\sqrt{\theta\pi}}{384(1+e)g_0}\left[1+\frac{6}{5}\varepsilon_{rbc}\,g_0(1+e)\right]^2+2\varepsilon^2{}_{rbc}\,\rho_{rbc}\,d_p\,g_0(1+e)\left(\frac{\theta}{\pi}\right)^{\frac{1}{2}} \tag{32}$$

Lastly, the energy dissipation, which is produced due to an inelastic collision of particles, was firstly defined in works of Savage [28] and is given by:

$$\gamma=\frac{12(1-e^2)\,g_0}{d_p\sqrt{\pi}}\varepsilon^2{}_{plt}\,\rho_{plt}\,\theta^{3/2} \tag{33}$$

$$\gamma=\frac{12(1-e^2)\,g_0}{d_p\sqrt{\pi}}\varepsilon^2{}_{rbc}\,\rho_{rbc}\,\theta^{3/2} \tag{34}$$

Chapter 4 – Results and Discussions

4.1. General description of the result comparison

Previous works prepared by Mendygarin et al. [4] and Supiyev et al. [6] permitted to simulate the blood flow in the capillary tube and found the peak PLT concentration 70mm far from the inlet, where it was determined the developed flow condition. This research will be evaluating the peak concentration at the same distance from the inlet.

To determine the effects of the VMF and Lift forces, several simulations were performed. First, the simulations were run only considering drag force, the same method used by Mendygarin et al [4]. At the next step, VMF and lift forces were added separately to observe their individual effect on the simulation. Lastly, both forces were added, and the final results were obtained. In this part of the report, results for all mentioned cases will be illustrated and the effect of the forces on peak PLT concentration will be scrutinized.

It was observed that VMF and lift force effects on the PLT concentration depend on the drag coefficient. In this work, two different drag coefficients were used.

In addition, drag coefficients for both RBCs and PLTs were chosen to be same and constant to reduce the number of variables.

4.2. Blood segregation model results with Cd=1

For this simulation the difference in mass flow between inlet and outlet was $2.08*10^{-3}$ %, which demonstrates the convergence of the results.

Figure 4.2.1 represents the volume fraction distribution of the RBC before application of the VMF and lift force:

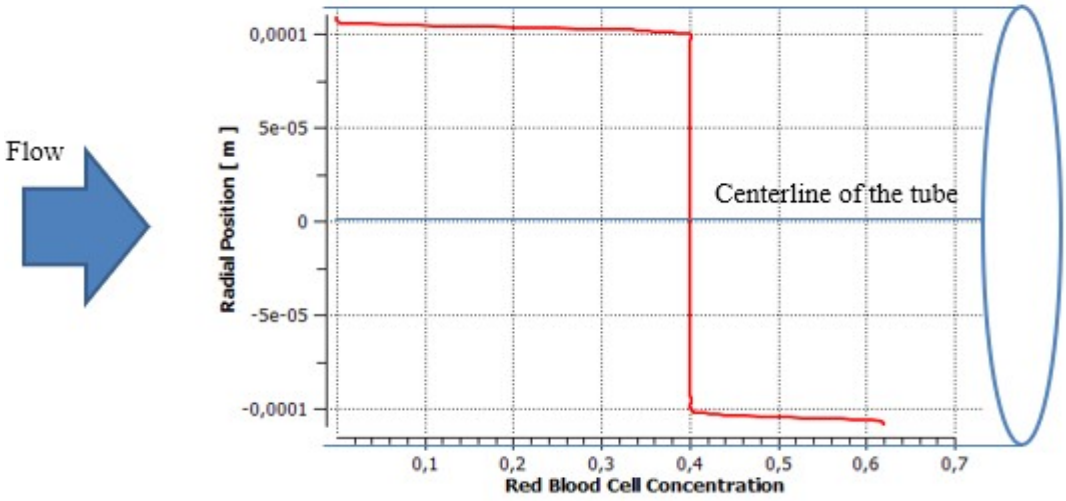

Figure 4.2.1. RBC concentration among the tube diameter

Radial position stands for a distance from the center of the pipe. The centerline of the tube is located at 0, the positive value is a distance from the centerline to an upper part of the tube. Consequently, the negative value of Radial position corresponds to the bottom side of the pipe.

As it can be seen from Figure 4.2.1. the RBCs are mainly located at the bottom part of the tube. That is because of high density and size of the RBC. The gravitational force affecting them, moves RBCs to the bottom part of the tube, driving plasma and PLT at the upper part of the tube. The abovementioned phenomenon can be seen in the following figure 4.2.2 and figure 4.2.3.

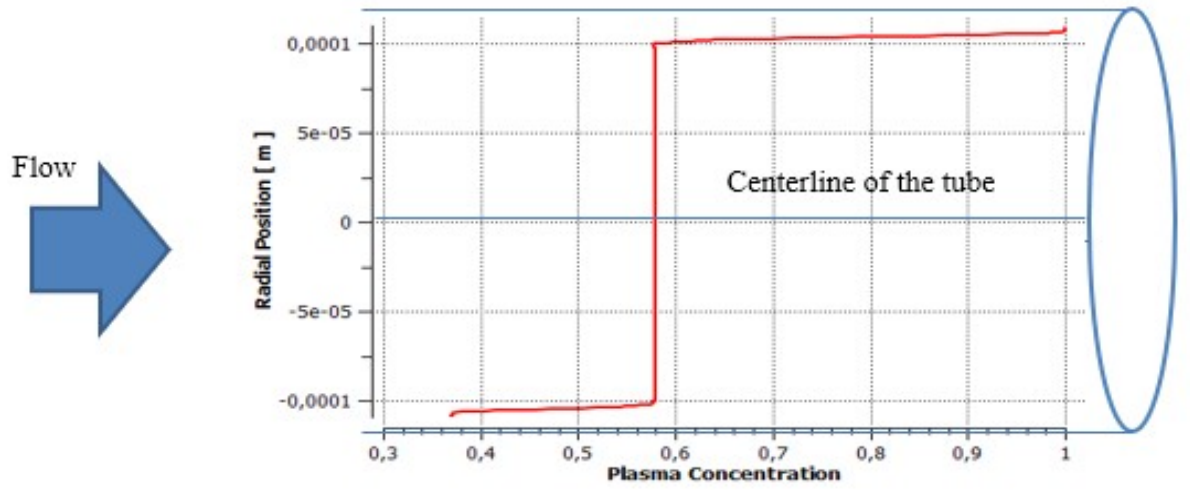

Figure 4.2.2. Plasma concentration among the tube diameter

Figure 4.2.3 shows the volume fraction of the PLTs inside the tube. From figure 4.2.3. it can be observed that PLT are highly concentrated at the upper part of the tube and the peak of the PLT concentration occurs at the region close to the upper wall of the tube.

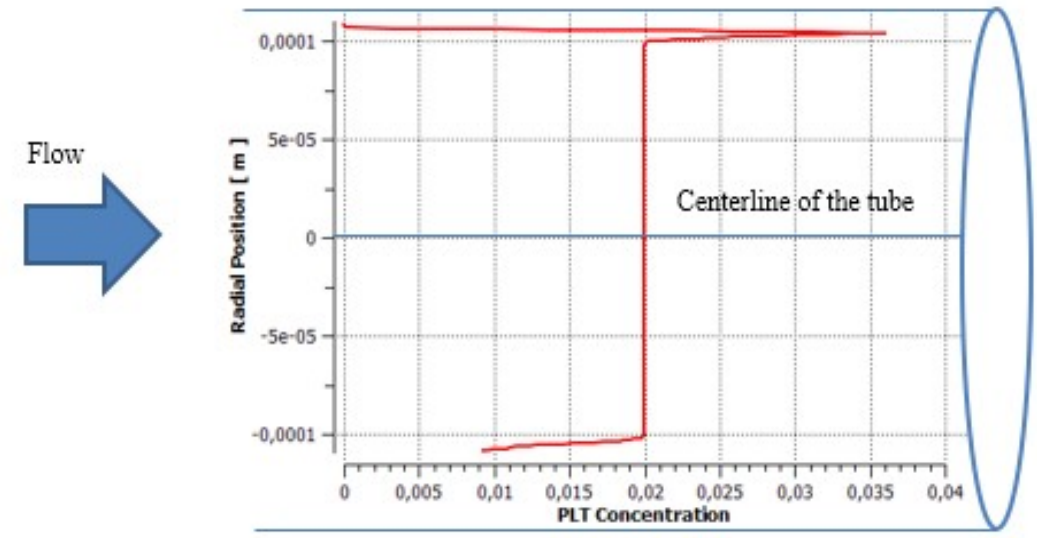

Figure 4.2.3. PLT concentration among the tube diameter

The same pattern of the blood cells distribution is observed for all simulations.

Now, to determine the relative concentration of the PLT, the local volume fraction will be divided to bulk volume fraction. Bulk one is fixed and equal to 0.02 or 2% of the total mixture. Figure 4.1.2. represents the relative PLT concentration at the position near the wall:

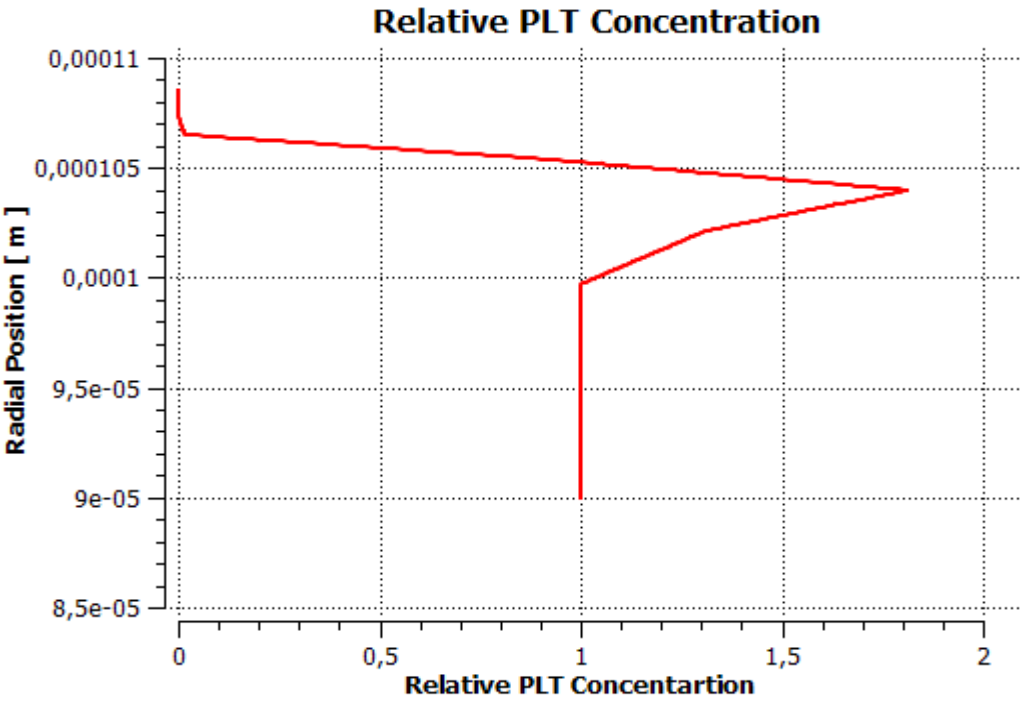

Figure 4.2.4. Peak Relative PLT concentration

It is important to mention that from Figure 4.1.2. the PLTs concentration are found to be at some distance from the wall, not at the wall itself. It demonstrates that the results are coincide with theory of F-L effect.

Now, the peak PLT concentrations evaluated for various force combinations will be illustrated in the tables 4.1 and 4.2.

For the first round of simulations the drag coefficient was set to $C_d = 1$. Effects of each force is shown in Table 4.1.

Table 4.2. Results of the peak PLT concentration for different force applications

VMF	Lift Force	Peak PLT Concentration
no	no	1,80
yes	no	1,815
no	yes	1,873
yes	yes	1,957

Table 4.1 illustrates that the effect of the VMF is very small comparing to lift force. However, in combination, the increase in PLT concentration was 8.7%. If we compare these results with ones obtained by Mendygarin et al. [4], the improvement is about 1%.

4.3. Blood segregation model results with C_d=5.5

For this simulation mass flow difference between inlet and outlet was equal to $2.673*10^{-3}$ %, showing the convergence of the results.

The following table represents the results of VMF and Lift force applications an drag coefficient of 5.5.

Table 4.3.1. Results of the peak PLT concentration for different force applications

VMF	Lift Force	Peak PLT Concentration
no	no	1.710
yes	no	1,712
no	yes	1,708
yes	yes	1,703

Effects of both forces were negligible and the final PLT concentration is lower than the original one.

The observations found a slight improvement of peak PLT concentration at a very low drag coefficient (C_d=1). With an increase in drag coefficient (C_d=5.5) the impact of the VMF and Lift force becomes negligible, and drag force become dominant.

All the figures representing the peak PLT concentrations for different set-ups (C_d=1) are included to the appendix section of the thesis. Since, the effect of the VMF and Lift force are negligible at C_d=5, the figures with relative PLT concentration at that drag coefficient are not included.

The following Table 4.3.2. presents the results obtained by different segregation models:

Table 4.3.2. Relative PLTs concentration by different models

Model	**Experimental data Yeh et al. [6]**	**Multiphase model Mendygarin et al. [4]**	**Multiphase model Ormanaliyev**
The peak of relative PLTs concentration	12	1.937	1.957
Equilibrium position y_e	0.98	0.96	0.96

where, the equilibrium position y_e is a distance between the peak PLT concentration and the centerline of the microtube.

Chapter 5 – Conclusion

This MSc thesis presents the results of an attempt to develop an improved blood segregation model in flow through a microtube. The aim of the thesis was to validate and simulate the experimental results obtained by Yeh et al. The work was based on findings developed previously by Mendygarin et al [4] and Supiyev et al [6] This study hypothesized that addition of the VMF and Lift force into the simulation should increase the peak PLT concentration and improve the blood cell segregation. The results of the simulations demonstrated the dependence of the VMF and Lift force effects on the drag coefficient. For very small drag coefficient the increase in the peak PLT concentration was about 8.7%. Moreover, the final peak value (1.96) was higher than one obtained by Mendygarin et al [4]. However, predicted peak PLT concentration is still very far from the experimental values.

Moreover, with increased drag coefficient the effect of both VMF and Lift force were negligible and did not affect the peak PLT concentration prediction. This additionally illustrates the complicated interrelations of the forces and their final effect on the blood cells segregation.

This study considered the spherical shape of the RBCs, which is a rough approximation. Although previous work of the Supiyev et al [6] showcased the reduction in the peak PLT prediction, authors believe that shape deformation of

the RBCs should be considered. Lift force is dependent on the shape of the particle and consideration of the shape irregularities might improve the current results.

Reference List

[1]. World Health Organization, "World health statistics 2017: monitoring health for the SDGs, Sustainable Development Goals". Geneva: Licence: CC BY-NC-SA 3.0 IGO. 2017

[2]. Di Terlizzi, R. "Hemolysis".

[3]. Rapido, F., "The potential adverse effects of haemolysis", Blood Transfus, 2017 May; 15(3): 218–221.
doi: [10.2450/2017.0311-16]

[4]. Mendygarin Y., Kussaiyn N., Luis R. Rojas-Solórzano, Zhussupbekov M., Supiyev R. , "Eulerian-Eulerian Multiphase Modeling of Blood Cells Segregation in Flow through Microtubes," ASME IMECE 2017 Proceedings, in press

[5]. Goldsmith H. L., G. R. Cokelet and P. Gaethgens, "Robin Fahraeus: evolution of his concepts in cardiovascular physiology", Received 8 November 1988; accepted in final form 16 May 1989.

[6]. Supiyev R., Luis R. Rojas-Solórzano, Mubita T. M., Zhussupbekov M., Zhanshayeva L., "CFD Multiphase Modeling of Blood Cells Segregation in Flow through Microtubes," AIDIC IBIC 2018, accepted abstract, full paper in progress.

[7]. Yeh, Chinjung, Anne C. Calvez, and Eugene C. Eckstein, "An estimated shape function for drift in a platelet-transport model," Biophysical journal 67.3: 1252-1259, 1994

[8]. Kolev, Nikolay I., "Multiphase Flow Dynamics 2 Thermal and Mechanical Interactions", 3rd Edition. 2007

[9]. Zhou, J., Giridhar, P. V., Kasper, S., & Papautsky, I., "Modulation of aspect ratio for complete separation in an inertial microfluidic channel". Lab on a Chip, 13(10), 2013, 1919. doi:10.1039/c3lc50101a

[10]. Zeng, L., Balachandar, S., & Fischer, P. "Wall-induced forces on a rigid sphere at finite Reynolds number". Journal of Fluid Mechanics, 2005, 536, 1–25. doi:10.1017/s0022112005004738.

[11]. Takemura, F., and J. Magnaudet. "The transverse force on clean and contaminated bubbles rising near a vertical wall at moderate Reynolds number". Journal of Fluid Mechanics, 495, 2003, 235–253. doi:10.1017/s0022112003006232

[12]. Massoudi, M. "On the importance of material frame-indifference and lift forces in multiphase flows". Chemical Engineering Science, 57(17), 2002, 3687–3701. doi:10.1016/s0009-2509(02)00237-3

[13] Goldsmith HL, Mason SG. Axial Migration of Particles in Poiseuille Flow. Nature 1961;190:1095.

[14]. Al-Taweel, A.M., S. Madhavan, K. Podila, M. Koksal, A. Troshko and Y.P. Gupta, "CFD Simulation of Multiphase Flow: Closure Recommendations for Fluid-Fluid Systems, 12th European Conference on Mixing", Bologna, Italy, June 27-30, 2006

[15]. Massoudi, M., J. Kim and J. F. Antaki,, "Modeling and numerical simulation of blood flow using the Theory of Interacting Continua", Published in final edited form as: Int J Non Linear Mech. 2012 Jun 1; 47(5), 2006: 506–520. Published online 2011 Sep 22.
doi: [10.1016/j.ijnonlinmec.2011.09.025]

[16]. Lamb H. Hydrodynamics, Dover, New York.1945

[17]. Bournaski E, "Numerical simulation of unsteady multiphase pipeline flow with virtual mass effect", Int. J. for Numerical Methods in Engineering, vol 34 pp 727-740, 1992

[18]. Kendoush, A. A., Sulaymon, A. H., and S. A. M. Mohammed, "Experimental evaluation of the virtual mass of two solid spheres accelerating in fluids". Experimental Thermal and Fluid Science, 31(7), 2007, 813–823. doi:10.1016/j.expthermflusci.2006.08.007
[19]. Fuat Yilmaz and Mehmet Yasar Gundogdu, "Analysis of conventional drag and lift models for multiphase CFD modeling of blood flow'. pp. 161-173. Korea-Australia Rheology Journal Vol. 21, No. 3, September. (Received July 1, 2009; final version received July 28, 2009)
[20]. Ishii, M. and T. Hibiki, "Thermo-fluid Dynamics of Twophase Flow", Springer, New York, 2006
[21]. Hibiki, T., and M. Ishii, Lift force in bubbly flow systems,
Chem. Eng. Sci. 62, 6457-6474, 2007.
[22]. Geislinger T.M. and T. Franke. "Hydrodynamic lift of vesicles and red blood cells in flow – from Fåhræus & Lindqvist to microfluidic cell sorting "
[23]. Saffman, P.G., "The lift force on a small sphere in a slow
shear flow", J. Fluid Mech. 22, 385-400, 1965.
[24]. Saffman, P.G., "Corrigendum to "The lift on a small sphere
in a slow shear flow", J. Fluid Mech. 31, 624,1968.
[25]. Mei, R., C.J. Lawrence and R.J. Adrian, "Unsteady drag on
a sphere at finite Reynolds number with small-amplitude fluctuations
in the free-stream velocity", J. Fluid Mech. 233, 613-631, 1991.
[26]. ***http://www.cvphysiology.com/Hemodynamics/H006***
[27]. Gidaspow, Dimitri, and Jing Huang, "Kinetic theory based model for blood flow and its viscosity," Annals of biomedical engineering 37.8: 1534-1545, 2009.
[28]. Savage, S. B. "Granular flow at high shear rates". In: Theory
of Dispersed Multiphase Flow, edited by R. E. Meyer. New York: Academic Press, 1983, pp. 339–358.

Appendix

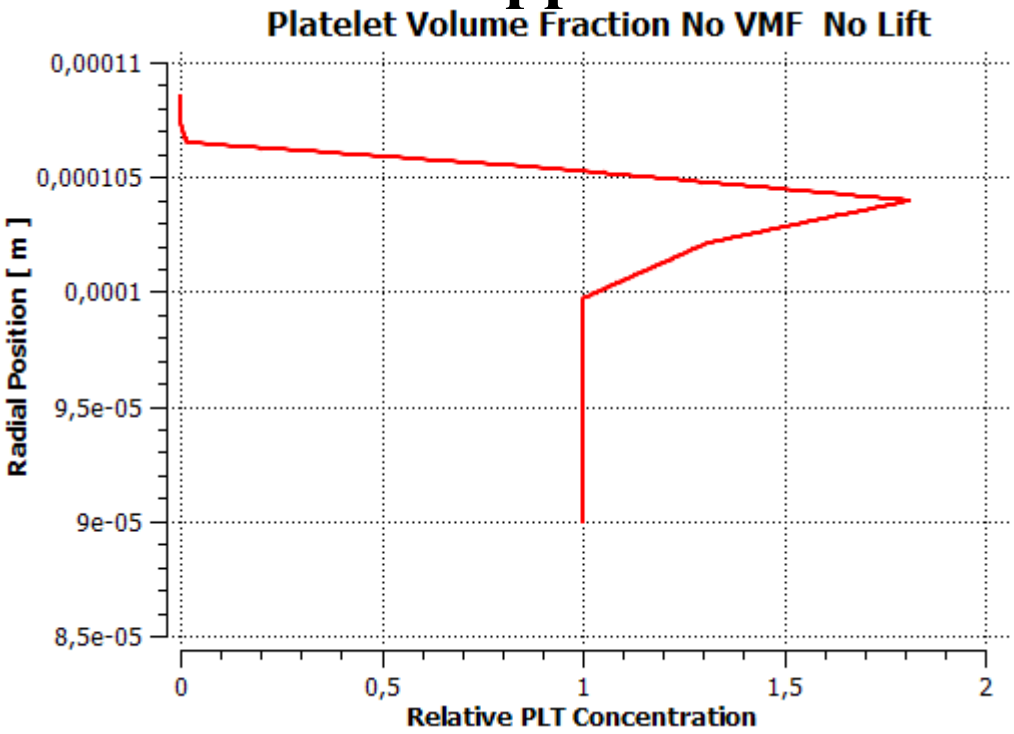

Figure 1. Relative PLT concentration without VMF and Lift

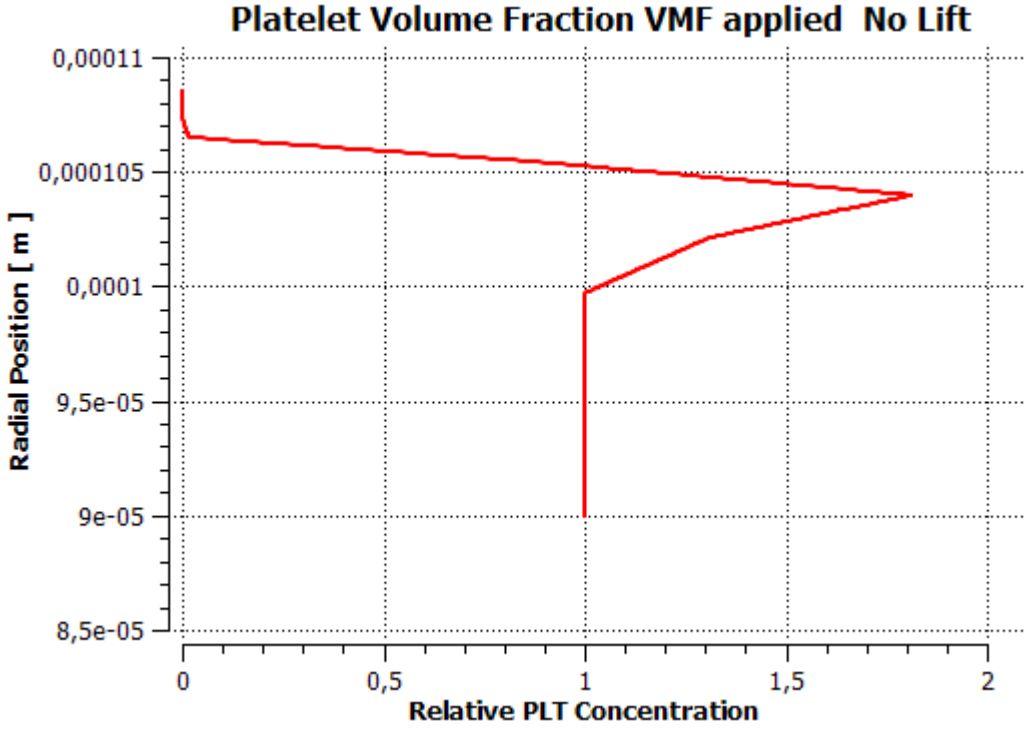

Figure 2. Relative PLT concentration: VMF applied and no Lift

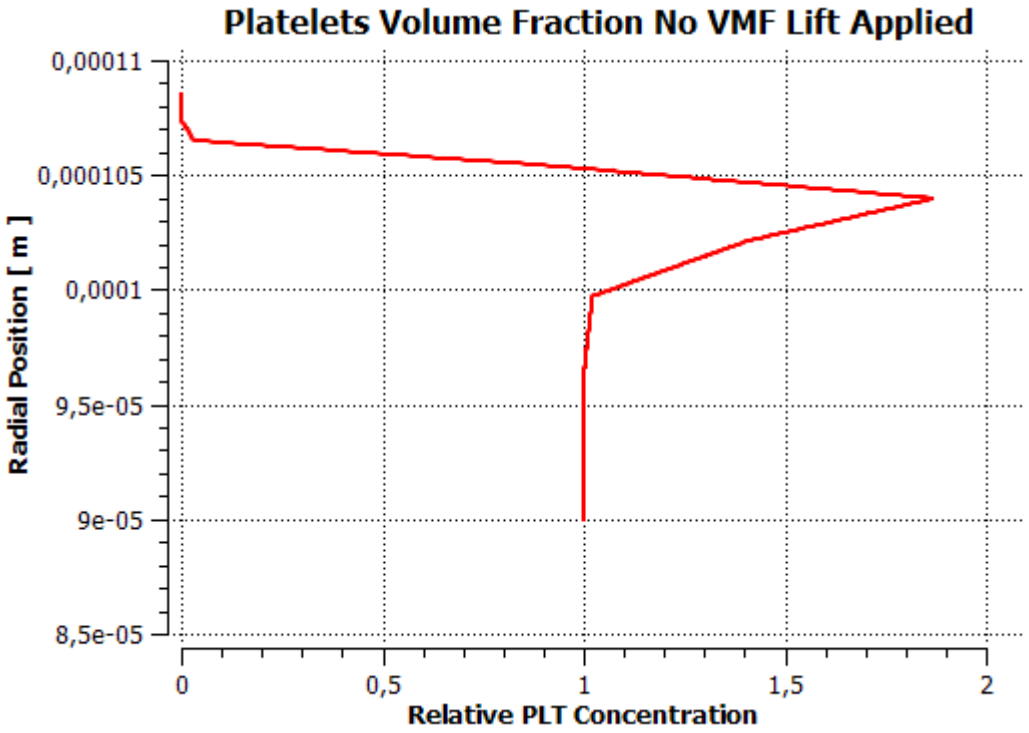

Figure 3. Relative PLT concentration without VMF and Lift applied

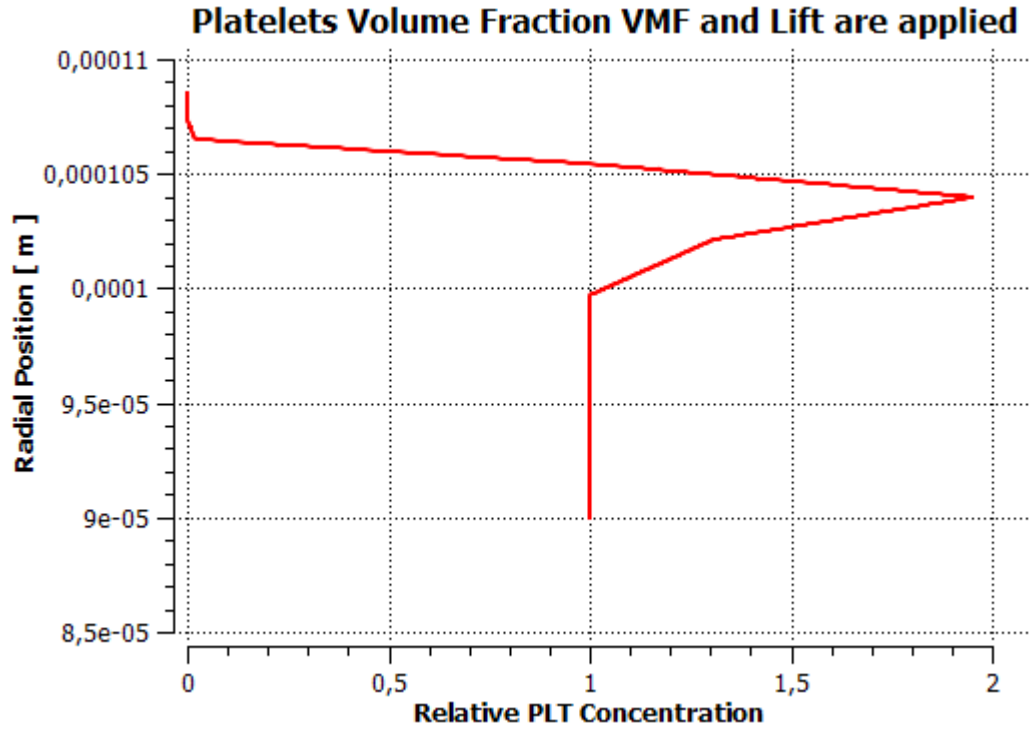

Figure 4. Relative PLT concentration with VMF and Lift applied